Joint Special Interest Group meeting between euspen and ASPE
Advancing Precision in Additive Manufacturing
KU Leuven, Belgium, September 2023
www.euspen.eu

Adaptive resolution two-photon 3D printing with X-ray tomographic resolution optimization of ultracompact 3D microfluidics

Markus Lunzer[1], A. Nelson Butterfield[2], Konstantinos Karpos[3], Christian M. Schlepütz[4], Richard Kirian[3], Michael Heymann[2]

[1]*UpNano GmbH, Austria*
[2]*Institute of Biomaterials and Biomolecular Systems, University of Stuttgart, Germany*
[3]*Department of Physics and The Biodesign Institute, Arizona State University, USA*
[4]*Swiss Light Source, Paul Scherrer Institute, Switzerland*

markus.lunzer@upnano.com

Abstract
Two-photon polymerization 3D printing (2PP) can build complex functional devices from submicron-scale volumetric units called voxels. However, 2PP is a comparably slow method for generating bulk volumes due to its exceptionally high-resolution: a small voxel is scanned in a line-by-line fashion, hence print time scales with volume. Faster printing can be achieved by increasing the rate of volume processed per time. This can be done by optical voxel enlargement: larger voxels can be spaced farther apart, thus fewer scan operations are required to polymerize a given volume resulting in faster print speeds, however, at the expense of print precision. Nevertheless, in adaptive resolution 2PP precision is only applied where structurally needed, increasing the throughput vastly.
We demonstrate this method on the example of ultracompact 3D microfluidic devices. Functional micro-nozzles are fabricated at different fine and coarse print settings and combinations thereof. For quality quantification we apply synchrotron X-ray tomography, which gives valuable insights on both external and internal micro-features as well as surface topography. In refining regional print settings and hence the local resolution to match performance requirements ultra-rapid fabrication of functional devices becomes possible. Such print time savings facilitate 2PP mass-production, as any loss in time is multiplied.

Adaptive control, 3D printing, Laser, Ultra-precision

1. Introduction

The ability to fabricate free-form 3D designs has greatly expanded the functionality of microfluidic devices when compared to previous 2D-lithography and injection molding-based microfluidics [1–3]. Two-photon polymerization (2PP) 3D-printing has the potential to build complex parts at sufficient precision to create functional microfluidic devices [4–6]. This proceeds by moving a focused pulsed-laser beam through a photosensitive resin, causing only the focal volume (voxel) to cure upon photoinitiation by near-simultaneous absorption of two photons, building up a 3D structure voxel line by voxel line, layer by layer [7, 8]. The nonlinearity of this process can even realize print features below the diffraction limit [5].

Unfortunately, 2PP 3D printing is a comparably slow method for generating bulk volumes: a small voxel is used to sequentially polymerize a target design, hence print time scales with design volume [5, 9, 10]. To increase the utility of this fabrication method, faster print speeds are needed to achieve high-throughput design iteration and batch production while minimizing costly machine runtime.

We increase 2PP throughput by dynamic voxel enlargement via optical modulation of the laser. Larger voxels can be spaced farther apart while still overlapping. The fewer scan operations thus required to polymerize a given volume results in higher throughput. However, increasing print speed by voxel enlargement comes at the expense of print precision, and in turn may impair device performance [3, 11–16].

The optimal print protocol thus uses the fastest print settings that still achieve sufficient precision to meet all local performance requirements. To identify this optimum requires an iterative cycle of part fabrication, measuring part precision and performance, and then using this information to adjust the print settings for the next iteration.

We apply this method to a gas dynamic virtual nozzle (GDVN) design for serial fs crystallography (Figure 1) [3, 17, 18, 19].

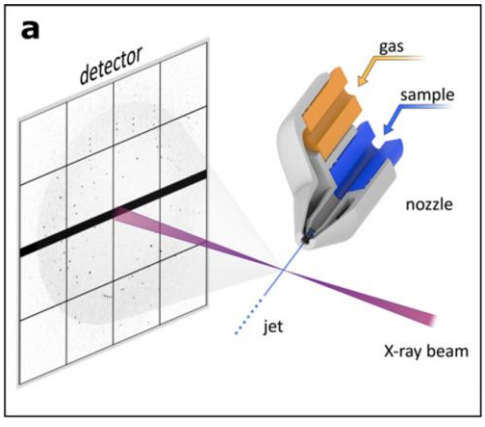

Figure 1. GDVN micro-nozzles are critical devices in serial fs-crystallography experiments. They focus a liquid stream with an outer sheath of inert gas to generate a fine liquid jet with a diameter of only a few µm [3]. Stable microjets are required to deliver a protein crystal slurry into the X-ray interaction region [20]. X-ray beam pulses are just tens of fs long, brief enough to allow diffraction of the crystals by high-intensity radiation before they are vaporized [21]. Thousands of diffraction patterns from separate, randomly oriented crystals are then combined to reconstruct the molecular 3D structure.

2. Methodology

2.1. 2PP 3D printing

Microfluidic nozzles can be manufactured by 2PP [4, 22]. The high-resolution 3D printing system NanoOne 1000 (UpNano GmbH) allows to fabricate parts in *vat* printing mode, in which a 780 nm fs-pulsed NIR laser (90 fs, 80 MHz) is focused trough a microscope objective (UPLXAPO10X, NA 0.4, Olympus) into a 2PP resin (UpDraft, UpNano GmbH) reservoir (Figure 2a). The voxel is scanned line by line (600 mm s^{-1} scanning speed), layer by layer, and maintained at a constant distance above the glass bottom, with the objective-vat unit moving away from the part as it grows. The voxel size and hence the resolution can be adapted by dynamic optical tuning (DOT). DOT is a method which, without changing the objective, optically modifies the laser focal point so that the voxel width is affected more strongly than the height, meaning that voxel widening decreases its aspect ratio. Thus, the print speed can be increased by lowering the voxel density, without overly compromising vertical resolution. In assigning the print settings (hatching, slicing) to local precision requirements, the throughput can be significantly increased compared to the conventional 2PP printing approach.

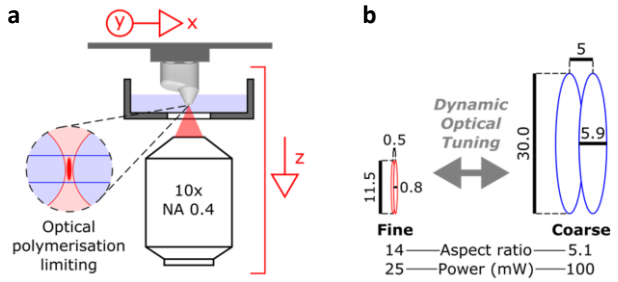

Figure 2. a) Principle of *vat* mode 2PP 3D printing. **b)** By adjusting voxel size and hatching distance, *fine* or *coarse* scan mode can be selected on the fly to match local precision requirements. Lengths in µm.

2.2. Synchrotron X-ray micro-tomography

A rational reduction of local print precision without impairing part performance requires suitable quantification of its functionally relevant 3D topography. X-ray microtomography can provide detailed 3D information of a scanned part, revealing both external and internal surfaces, which can be directly compared to the corresponding CAD design in silico (Figure 3). The precision can be measured using "fidelity", which quantifies the normal surface deviation of the printed part from the target CAD file, which depending on the resolution, can be done at sub-micrometre precision. X-ray rotation series of mounted samples, comprising 2001 images over an 180° rotation sweep, were collected at the TOMCAT beamline of the Swiss Light Source at Paul Scherrer Institute (Villigen, CH). A 12 keV X-ray energy and a 6 mm separation between sample and scintillator (20 µm thick LuAG:Ce (Crytur)) yielded optimal X-ray absorption contrast and edge enhancement for phase contrast reconstruction and part segmentation. Resulting deviation maps can now inform detailed print process optimizations.

2.3. Jet tests

Jet tests [23] were conducted using a custom station controlled by an open-source python package which automated the collection and analysis of data [18 ,23]. A GDVN was mounted horizontally into a ~4x4x10 cm vacuum chamber (0.1 mbar) connected to an Edwards XDS35 scroll pump. Jets were illuminated with pulsed diode laser (633 nm, DILAS D4F4S22 with a custom current driver) and imaged with a Photron SA5 high-speed camera connected to Mitutoyo 10x M Plan Apo long-working-distance objective and a Navitar Ultra-Zoom 12x lens. The liquid flow was controlled by a LD-20AD Shimadzu HPLC pump and measured with a SLI-0430 Sensirion flow sensor. The helium mass mass flow rate was measured and controlled by an EL-FLOW Bronkhorst controller.

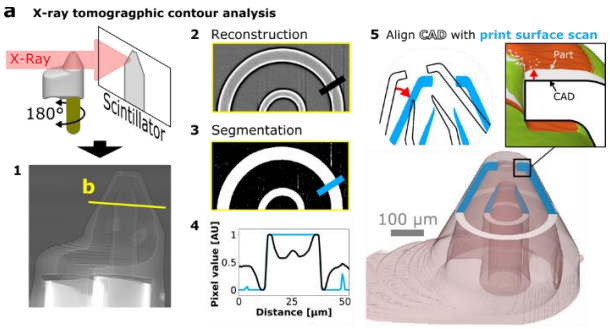

Figure 3) High-resolution 3D print quality quantification via X-ray tomography. Tomographic scans acquired 180° rotation series (1) using a 12 keV X-ray synchrotron beam in phase contrast mode. Paganin phase contrast tomogram reconstruction (2) was used to facilitate segmentation (3) without degrading part edge precision (4). Segmented contours (5) of printed parts (blue) were aligned to their CAD mesh (black) to compute fabrication fidelity as the normal deviation of part surface from the original CAD instruction. While SEM is limited to viewing surface features, µCT can quantify fidelity and noninvasively reveal internal features.

3. Results and discussion

Voxel width was directly quantified via scanning electron microscopy (SEM) of single-voxel line prints (Figure 4a). Unmodified fine voxels had dimensions of XY = 0.5-1.1 µm, Z = 6.0-12.4 µm for the laser power range of 20-30 mW (red). Coarse voxels enlarged by dynamic optical tuning had dimensions of XY = 4.7-6.4 µm, Z = 15.9-39.3 µm for the laser power range 50-150 mW (blue). Voxel enlargement allows

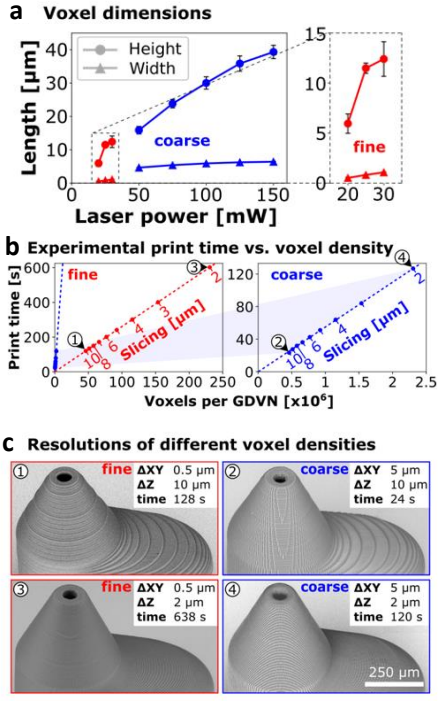

Figure 4) Adaptive resolution acts as virtual objective changer and permits *fine* and enlarged *coarse* voxel print modes. Voxel enlargement by dynamic optical tuning allows larger hatching and slicing distances, and thus faster print speeds by extending the lower limit of attainable voxel density.

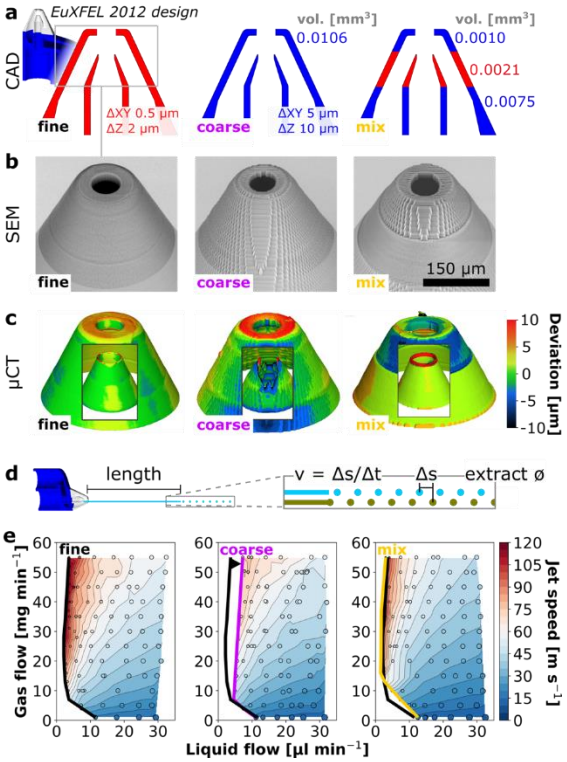

Figure 5) Performance dependent fidelity guides print speed optimisation of EuXFEL GDVN.

larger hatching and slicing distances, and thus faster print speeds by extending the lower limit of attainable voxel density (Figure 4b). Electron microscopy reveals the effect of different print settings on resolution, and confirms the structural viability of larger voxel spacing (Figure 4c). The EuXFEL2012 GDVN design, with an overall volume of ~0.1153 mm^3, printed solid with 10 µm ΔZ_{scan} slicing, took 128 s to print in *fine* and only 24 s in *coarse* mode, corresponding to a 246-fold faster print speed compared to the 98.5 min previously required to print a GDVN of comparable size using the default solid setting of a Nanoscribe Photonics Professional GT [19].

Next, the EuXFEL2012 design was divided into regions of different *fine* and *coarse* print settings, with higher print speeds used where the lower precision doesn't impair functionality (e.g. nozzle body). The effect of each print setting (*fine tip, coarse tip, mix tip*) illustrated in Figure 5a was revealed by scanning electron microscopy (Figure 5b) and microtomography-enabled fidelity quantification (Figure 5c). GDVN performance was characterized by jet measurements of length, speed and diameter, which are collected by analysing jet images using a custom python code (Figure 5d) and converted into representative phase diagrams showing the jet speeds and diameters (reflected by marker size) for different gas and liquid flow combinations (Figure 5e). The left edges of these diagrams, delineated with bold lines, represent the drip-to-jet boundaries, which deteriorated markedly for coarse voxel mode printed nozzles.

By spatially varying voxel resolution according to functional demand, nozzle fabrication time was greatly reduced without compromising performance. Coarse mode (blue) achieves 15-fold faster fabrication rates then fine (red) mode (Figure 6a). Overall, fabrication speeds are hence highly sensitive to the volume fraction allocated to slow fine mode printing. While the all *coarse* and all *fine* nozzles achieved quite different lowest jet flow rates (Figure 5e), they all performed sufficiently well for routine serial crystallography experiments. Axis-specific print defects in the *coarse* mode inner nozzle, however, did not impair orifice symmetry and alignment centricity, which may explain the minimal impact on jetting performance (Figure 5c). In contrast, conventional hand-made glass capillaries are more likely to suffer from pronounced jet whipping due to misaligned inner liquid and outer gas orifice impairing performance. The most critical section in the EuXFEL2012 nozzle was identified as the inner orifice, allowing us to limit the fine mode high resolution sections to this small feature, comprising 1.7 volume percent of the full nozzle taking 20 s to print in fine mode, compared to the remaining 98.3 volume percent completing in 24 s coarse mode printing (mix tip in Figure 5 and 6). The total print time of the mixed tip nozzle (41 s) results in a 144-fold increase compared to the previously required print speed of a GDVN of that size (98.5 min) [19].

Due to this tremendous increase in throughput batch production becomes reasonable. 392 nozzles have been fitted onto a 20x20 substrate, 2 of each in a 1.4 x 1.4 mm^2 FoV to compensate for additional stage movement, and can now be fabricated by 2PP within 5 h 20 min in parallel, resulting in an individual nozzle print time of 49 s.

5. Conclusion

We increase 2PP print speed by lowering the number of voxels to be printed, enabled by enlarging these voxels. Moreover, we optimise these new print settings in terms of fidelity and functionality by using X-ray tomography and automated phase diagram collection, respectively, thus establishing an optimisation protocol. Applying a combination of the optimized print settings increased the throughput 144-fold, which allowed to bulk produce 392 pieces of a highly complex hypodermic needle GDVN in less than 5.5 hours.

The presented fidelity optimisation protocol could prove invaluable to other microscopic devices. Micro- and even nanometre deviations are relevant in optics, for example, making this an option for optimising fabrication of microscopic lenses [24–27] and biomimetic eyes [28].

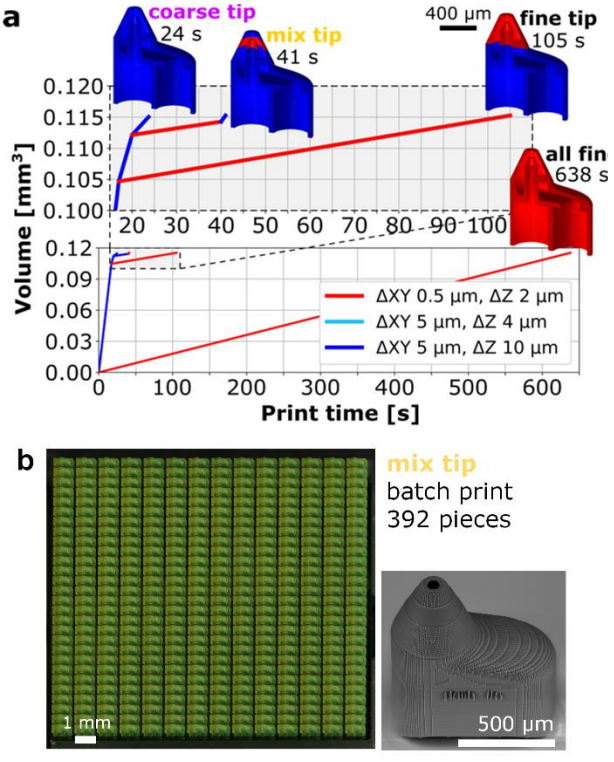

Figure 6) Device performance optimized resolution and fabrication rates allows in significant throughput increase which allows large scale batch production (392 pcs) within reasonable print time.

References

[1] Nielsen A V, Beauchamp M J, Nordin G P, Woolley A T 2020 3D Printed Microfluidics *Front. Nanotechnol.* **3** 609355

[2] Bhattacharjee N, Urrios A, Kang S, Folch A 2016 The upcoming 3D-printing revolution in microfluidics. *Lab. Chip.* **16** 1720–1742

[3] Nelson G et al. 2016 Three-dimensional-printed gas dynamic virtual nozzles for x-ray laser sample delivery. *Opt Express.* **24** 11515

[4] Maruo S, Nakamura O, Kawata S 1997 Three-dimensional microfabrication with two-photon-absorbed photopolymerization *Opt. Lett.* **22** 132-134

[5] Farsari M, Chichkov B N 2009 Two-photon fabrication. *Nature Photon*. **3** 450–452

[6] McLennan H J, Blanch A J, Wallace S J, Ritter L J, Heinrich S L, Gardner D K, Dunning K R, Gauvin M J, Love A K, Thompson J G 2023 Nano-liter perfusion microfluidic device made entirely by two-photon polymerization for dynamic cell culture with easy cell recovery *Sci. Rep*. **13** 562

[7] Ligon S C, Liska R, Stampfl J, Gurr M, Mülhaupt R 2017 Polymers for 3D Printing and Customized Additive Manufacturing *Chem. Rev.* **117** 10212–10290

[8] Song J, Michas C, Chen C S, White A E, Grinstaff M W 2020 From Simple to Architecturally Complex Hydrogel Scaffolds for Cell and Tissue Engineering Applications: Opportunities Presented by Two-Photon Polymerization *Adv Healthcare Mater.* **9** 1901217

[9] Zhou X, Hou Y, Lin J 2015 A review on the processing accuracy of two-photon polymerization *AIP Adv.* **5** 30701

[10] Barner-Kowollik C, Bastmeyer M, Blasco E, Delaittre G, Müller P, Richter B, Wegener, M. 2017 3D Laser Micro- and Nanoprinting: Challenges for Chemistry *Angew. Chem. Int. Ed.* **56** 15828–15845

[11] Keller M, Czilwik G, Schott J, Schwarz I, Dormanns K, Von Stetten F, Zengerle R, Paust N 2017 Robust temperature change rate actuated valving and switching for highly integrated centrifugal microfluidics. *Lab. Chip*. **17** 864–75

[12] Jia J, Song Q, Liu Z, Wang B. 2019 Effect of wall roughness on performance of microchannel applied in microfluidic device *Microsyst Technol.* **25** 2385–2397

[13] Villegas M, Cetinic Z, Shakeri A, Didar T F 2018 Fabricating smooth PDMS microfluidic channels from low-resolution 3D printed molds using an omniphobic lubricant-infused coating *Analytica Chimica Acta.* **1000** 248–225

[14] Zahoor R, Bajt S, Šarler B 2018 Influence of Gas Dynamic Virtual Nozzle Geometry on Micro-Jet Characteristics *Int. J. Multiphase Flow* **104** 152–65

[15] Rubio A, Rodríguez S, Cabezas M G 2020 Capabilities and Limitations of Fire-Shaping to Produce Glass Nozzles. *Materials* **13** 5477

[16] Hejazian M, Balaur E, Abbey B 2021 Recent Advances and Future Perspectives on Microfluidic Mix-and-Jet Sample Delivery Devices *Micromachines* **12** 531

[17] Wiedorn M O, et al. 2018 Megahertz serial crystallography *Nat. Commun*. **9** 4025

[18] Nazari R, Zaare S, Alvarez R C, Karpos K, Engelman T, Madsen C, Nelson G, Spence J C H, Weierstall U, Adrian R J, Kirian R A 2020 3D printing of gas-dynamic virtual nozzles and optical characterization of high-speed microjets *Opt. Express.* **28** 21749

[19] Knoška J et al. 2020 Ultracompact 3D microfluidics for time-resolved structural biology *Nat. Commun.* **11** 657

[20] DePonte D P, Weierstall U, Schmidt K, Warner J, Starodub D, Spence J C H, Doak, R B 2008 Gas dynamic virtual nozzle for generation of microscopic droplet streams. *J. Phys. D: Appl. Phys.* **41** 195505

[21] Chapman H N 2011 Femtosecond X-ray protein nanocrystallography *Nature.* **470** 73–77

[22] Stampfl J, Liska R, Ovsianikov A 2016 Multiphoton Lithography: Techniques, Materials and Applications, Weinheim, (Wiley-VCH Verlag GmbH & Co. KGaA)

[23] Nazari R, Ansari A, Herrmann M, Adrian R J, Kirian R A 2023 Numerical and experimental investigation of gas flow field variations in three-dimensional printed gas-dynamic virtual nozzles *Front. Mech. Eng.* **6** 958963

[24] Thiele S, Arzenbacher K, Gissibl T, Giessen H, Herkommer A M 2017 3D-printed eagle eye: Compound microlens system for foveated imaging *Sci. Adv.* **3** 1602655

[25] Asadollahbaik A, Thiele S, Weber K, Kumar A, Drozella J, Sterl F, Herkommer A M, Giessen H, Fick J 2020 Highly Efficient Dual-Fiber Optical Trapping with 3D Printed Diffractive Fresnel Lenses *ACS Photonics* **7** 88–97

[26] Herkommer A M, Pruss C, Giessen H., Thiele S 2019 3D printed stacked diffractive microlenses. *Opt. Express* **27** 35621-35630

[27] Li J, et al. 2022 3D-Printed Micro Lens-in-Lens for In Vivo Multimodal Microendoscopy *Small* **18** 2107032

[28] Dai B, et al. 2021 Biomimetic apposition compound eye fabricated using microfluidic-assisted 3D printing *Nat. Commun.* **12** 6458